Kobe University Repository : Kernel

PDF issue: 2026-10-05

Summer carbon budget simulation in a lagoon ecosystem with submerged aquatic vegetation

Fukuda, Y. ; Maruyama, M. ; Peng, Y. ; Yoneda, H. ; Tada, K. ; Nakayama, K.

(Citation)
Science of The Total Environment,1043:181920

(Issue Date)
2026-08-10

(Resource Type)
journal article

(Version)
Version of Record

(Rights)
© 2026 The Authors. Published by Elsevier B.V.
This is an open access article under the Creative Commons Attribution 4.0 International license

(URL)
https://hdl.handle.net/20.500.14094/0100505527

Science of the Total Environment 1043 (2026) 181920

Contents lists available at ScienceDirect

Science of the Total Environment

journal homepage: www.elsevier.com/locate/scitotenv

Summer carbon budget simulation in a lagoon ecosystem with submerged aquatic vegetation

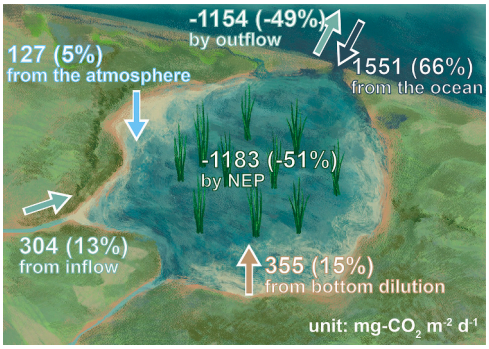
Y. Fukuda [a], M. Maruyama [a], Y. Peng [a], H. Yoneda [a], K. Tada [b], K. Nakayama [a,*]

[a] Graduate School of Engineering, Kobe University, 1-1 Rokkodai-cho Nada-ku, Kobe city, 658-8501, Japan
[b] Oriental Consultants, Co., Ltd., 3-2-18 Nakanoshima, Kita-ku, Osaka, 530-0005, Japan

HIGHLIGHTS

- New DIC model developed for eelgrass considering light and temperature
- Eelgrass significantly affects DIC dynamics in the lagoon by 300 μmol kg^{-1}
- Neglecting TA leads to several-fold overestimation of atmospheric CO_2 uptake
- Tides contribute 66% of CO_2 supply, while air-water flux accounts for only 6%
- Eelgrass absorbs 50% of the CO_2 supplied from the open ocean and river water

GRAPHICAL ABSTRACT



ARTICLE INFO

Keywords:
Photosynthesis
Respiration
Net ecosystem production
SAV
Blue carbon

ABSTRACT

As international efforts against global warming advance, blue carbon has gained attention as a CO_2 sink. This study quantitatively evaluated the carbon budget of an eelgrass (*Zostera marina*) ecosystem in Komuke Lagoon, a restricted coastal lagoon on the northeastern coast of Hokkaido, Japan. Based on outdoor experiments conducted in 2018 and 2023, a new DIC equation was constructed that incorporates photosynthetic responses to photon flux density and water temperature. Furthermore, a box model integrating river inflow, seawater exchange with the open ocean, air–water CO_2 flux, bottom dilution, and absorption by eelgrass was developed to reproduce the seasonal variations of DIC in the lagoon. The results demonstrated that excluding eelgrass led to a summer-validated overestimation, projected on an annual basis, of DIC by a maximum of approximately 300 μmol kg^{-1}, indicating that eelgrass significantly affects DIC dynamics. Additionally, ignoring variations in Total Alkalinity (TA) in the simulation resulted in an underestimation of pCO_2 by up to 150 μatm, potentially leading to a several-fold overestimation of atmospheric CO_2 uptake. Analysis of the summer-validated carbon budget, integrated over the simulated calendar year 2018, indicated that CO_2 supply from the open ocean via tides was the most dominant factor, contributing approximately 66%. While eelgrass absorbed about half of the CO_2 supplied to the lagoon, atmospheric CO_2 uptake accounted for only about 5.4% of the total. This study demonstrated that for carbon budget evaluation in highly enclosed shallow coastal areas, it is important to utilize modeling that considers flow and water exchange processes associated with river inflow and tides, as well as TA variations. Simulations for 2013 and 2019 were additionally performed as reproducibility and inter-annual consistency

* Corresponding author at: Graduate School of Engineering, Kobe University, 1-1 Rokkodai-cho Nada-ku, Kobe city, 658-8501, Japan.
E-mail address: nakayama@phoenix.kobe-u.ac.jp (K. Nakayama).

https://doi.org/10.1016/j.scitotenv.2026.181920
Received 9 January 2026; Received in revised form 25 May 2026; Accepted 26 May 2026
Available online 10 June 2026
0048-9697/© 2026 The Authors. Published by Elsevier B.V. This is an open access article under the CC BY license (http://creativecommons.org/licenses/by/4.0/).

checks against available summer observations; their full-year DIC trajectories are reported only as model projections, and the detailed carbon-budget partitioning reported here refers exclusively to 2018.

1. Introduction

Global warming is causing floods and droughts worldwide, making the mitigation of global warming an urgent task (IPCC, 2007; IPCC, 2013). As a countermeasure, CO_2 uptake by blue carbon ecosystems, such as seagrass meadows, is being promoted globally (Nellemann et al., 2009). Seagrass meadows, a representative blue carbon ecosystem, function to store autochthonous carbon (derived from seagrass growth) and allochthonous carbon as carbon stock in the seabed (Fourqurean et al., 2012). The high carbon sequestration capacity of these ecosystems is driven by both biological and physical mechanisms. Physiologically, seagrasses fix dissolved inorganic carbon (DIC) into organic matter through high rates of primary production. Physically, the complex three-dimensional structure of the seagrass canopy significantly dampens wave energy and reduces current velocity, which promotes the deposition of suspended organic particles from both internal and external sources (Duarte et al., 2013). Once these organic materials are trapped within the sediments, the typically anoxic conditions prevent rapid microbial decomposition, enabling the long-term storage of carbon over centennial to millennial timescales (Macreadie et al., 2019). However, the relative contributions of these biological-physical couplings to the dissolved carbon budget remain poorly quantified, particularly in enclosed lagoons where tidal and riverine forcing modify the dissolved inorganic carbon pool. The present study addresses this gap using a lagoon-scale box model constrained by outdoor experiments. In blue carbon ecosystems, CO_2 sequestered through photosynthesis by marine organisms is estimated to account for 55% of the carbon stored by living organisms on Earth, known as "green carbon" (Nellemann et al., 2009).

Despite being a blue carbon ecosystem with such a significant CO_2 sequestration effect, several unresolved issues must be addressed for a high-precision evaluation of CO_2 uptake. For instance, Short and Neckles (1999) indicated that since water depth and flow variations affect seagrass growth, it is necessary to estimate CO_2 uptake taking these factors into account. Additionally, Nakayama et al. (2020) demonstrated that utilizing numerical simulations that consider flow enables the reproduction of CO_2 uptake with high temporal resolution. Palacios and Zimmerman (2007) suggested the possibility that high atmospheric partial pressure of carbon dioxide (pCO_2) concentrations could increase CO_2 uptake and improve productivity in seagrass meadows. However, detailed analyses regarding the interaction between flow and photosynthesis-driven CO_2 uptake in seagrass meadows have not been conducted. Consequently, the impacts of river inflow, seawater exchange with the open ocean, and air-water CO_2 flux on CO_2 uptake in seagrass meadows remain unresolved.

To quantitatively evaluate the CO_2 uptake by seagrass meadows while considering flow effects, it is necessary to consider the mutual interference between flow and the seagrass meadows. This requires analyzing the partial pressure of CO_2 in water. It is necessary to select four elements from water temperature, salinity, Total Alkalinity (TA), Dissolved Inorganic Carbon (DIC), and pH, and to derive pCO_2 via chemical equilibrium equations (Zeebe and Wolf-Gladrow, 2001). Since analyzing water temperature and salinity is essential for numerical simulations in blue carbon ecosystems, two parameters remain to be selected. If chemical reactions of calcification and biological reactions are negligible, TA can be easily treated as a conservative substance similar to salinity and should be used in the numerical simulation. The remaining parameter should be DIC, which is a component directly absorbed through photosynthesis and plays a crucial role in calculating the carbon budget. Since DIC increases or decreases due to respiration and photosynthesis in addition to advection and diffusion, these processes must be modeled. As methods for evaluating DIC uptake by seagrass, the Arrhenius equation, which can consider the effect of water temperature, and the Jassby-type equation, which can reproduce CO_2 uptake via photosynthesis, are frequently used (Staehr and Borum, 2011; Beca-Carretero et al., 2018; Burkholz et al., 2019). Notably, the Jassby-type equation is found to fit not only laboratory experiment results but also field experiments (Drew, 1979; Goodman et al., 1995; Holmer and Bondgaard, 2001; Marsh Jr. et al., 1986; Olesen and Sand-Jensen, 1993; Touchette, 1999; Zimmerman et al., 1995; Zimmerman et al., 1997). In past research, the growth rate due to photosynthesis using photon flux density for eelgrass (*Zostera marina*) has been investigated in many previous studies (please see the review by Lee et al., 2007). The equation combining the Arrhenius equation and the Jassby-type equation is called the "DIC equation" (Nakayama et al., 2020).

On the other hand, regarding CO_2 uptake in blue carbon ecosystems considering flow, there is an application example of numerical simulation by Nakayama et al. (2022). They utilized the results of 3D numerical calculations in Cigu Lagoon to evaluate the seawater exchange flux between Cigu Lagoon and the open ocean with high precision. By treating Cigu Lagoon as a single box, it became possible to consider the interaction with flow, and they successfully quantitatively evaluated the CO_2 uptake by phytoplankton while considering the influence of oysters. The model that treats the target area as a single box has also been used to analyze the generation and dissipation of hypoxic water masses, and has successfully reproduced Dissolved Oxygen concentrations that recover rapidly due to strong winds (Nakayama et al., 2010; Sato et al., 2012). In blue carbon ecosystems, the model treating the target area as a single box is called a "conceptual DIC model." This model allows for the individual evaluation of river inflow, seawater exchange flux with the open ocean, CO_2 flux at the water surface, and CO_2 uptake by seagrass meadows. Furthermore, it was shown that in Cigu Lagoon, variations in TA are important and significantly affect the internal CO_2 uptake.

Therefore, in this study, we targeted the eelgrass meadows in Komuke Lagoon, an enclosed water body, to analyze the effects of river inflow, seawater exchange with the open ocean, and air-sea CO_2 flux on CO_2 uptake by the eelgrass meadows. First, to quantitatively evaluate the extent of CO_2 absorption by eelgrass, we determined the parameters of the DIC equation. For parameter determination, laboratory experiments were conducted using local eelgrass, utilizing direct measurements of water temperature, photon flux density, and pCO_2, as well as measurement results of DIC and TA obtained via water sampling (Nakayama et al., 2020; Maruyama et al., 2024). To reproduce temporally high-precision DIC and pCO_2, we constructed a "conceptual DIC model" treating Komuke Lagoon as a single box, which showed a good agreement with the field observations in 2018. We then quantitatively evaluated the influence of river inflow, seawater exchange with the open ocean, and air-sea CO_2 flux on CO_2 uptake by the eelgrass meadows. In doing so, we also examined the influence of TA on the CO_2 flux at the water surface.

The objective of this study is to provide a quantitative partitioning of the carbon budget in an eelgrass-dominated lagoon, building upon the modeling framework established by Nakayama et al. (2020). However, this study differs from previous efforts in four fundamental aspects that represent its key innovations. First, we have refined the DIC equation by replacing the simple Arrhenius-based photosynthesis model used in Nakayama et al. (2020) with a Jassby-type equation that incorporates both light saturation and temperature limitation. This modification accounts for the observed decline in photosynthetic efficiency at temperatures exceeding the optimum for *Zostera marina*. Second, this model explicitly incorporates the CO_2 exchange flux across the air-water

interface, which was previously neglected, allowing for a more comprehensive assessment of the lagoon's role as an atmospheric carbon sink. Third, we introduce the modeling of Total Alkalinity (TA) to account for its impact on carbonate equilibrium. By doing so, we aim to demonstrate the critical importance of TA variability—often driven by riverine dilution in enclosed coastal systems—in accurately calculating pCO_2 and preventing the significant overestimation of atmospheric CO_2 uptake. Fourth, simulations for 2013 and 2019 were additionally performed as a reproducibility test of the calibrated DIC equation and as an inter-annual consistency check of the conceptual DIC model, broadening the temporal scope beyond the single-campaign dataset used in Nakayama et al. (2020). The detailed quantitative partitioning of the carbon budget—summer-validated and integrated over the simulated calendar year of 2018—namely the relative contributions of river inflow, tidal exchange, bottom dilution, air–water CO_2 flux, and eelgrass metabolism—was conducted exclusively for 2018, the year for which simultaneous field observations of DIC, TA, salinity and laboratory photosynthesis experiments most densely constrain the model. Because all in-situ validation data are from summer (July–August), the simulated DIC dynamics outside of summer are reported as model projections only. Through these advancements, this study provides a high-precision evaluation of the lagoon-integrated carbon budget of a blue carbon ecosystem.

2. Method

2.1. Study site

Komuke Lagoon is located on the northeastern coast of Hokkaido, Japan (44°15′30“ N, 143°30’20” E), which connects to the Sea of Okhotsk through a tidal inlet and has a surface area of 3.8×10^6 m^2 and a volume of 3.33×10^6 m^3 (Fig. 1). The mean water depth is 1.2 m, and the qmaximum depth is 3.8 m. Komuke Lagoon consists of three enclosed basins and functions as a typical nutrient-trapping lagoon. While the tidal range in the Sea of Okhotsk is approximately 1 m, it is attenuated to only 0.5 m within the lagoon due to the narrow tidal inlet (width: 15 m). Consequently, calm water conditions prevail in Komuke Lagoon, supporting a wide distribution of eelgrass meadows that contribute to organic carbon sequestration in the sediments (Watanabe and Kuwae, 2021). The salinity ranges from approximately 20 to 34, driven by seawater exchange with the Sea of Okhotsk, exceeding river inflow. Furthermore, mean concentrations of nitrate nitrogen, ammonium nitrogen, and phosphate phosphorus were observed to be approximately 0.0033 mg L^{-1}, 0.0048 mg $L^{-1,}$ and 0.032 mg L^{-1}, respectively, from spring to autumn. Chlorophyll *a* (Chl. *a*) concentration is low at approximately 3 μg L^{-1}, indicating that the influence of phytoplankton on carbon absorption is negligible. Therefore, Komuke Lagoon is an ideal site for investigating the stratification effect on carbon absorption by SAV meadows.

Komuke Lagoon represents a geomorphically stable “restricted lagoon” as defined by Kjerfve (1994), a category that encompasses many seagrass-hosting coastal systems globally. Its narrow 15-m inlet effectively acts as a dynamic filter for oceanic tidal energy, reducing the tidal range within the lagoon to approximately 50% of that in the open Sea of Okhotsk. These hydrodynamically calm conditions, combined with relatively low phytoplankton biomass (Chl. a ~ 3 μg L^{-1}), ensure high water clarity and minimal physical disturbance. Within the global spectrum of blue carbon ecosystems, Komuke Lagoon serves as an ideal representative site for “choked” or “restricted” lagoons where the physical environment maximizes the biological carbon sequestration potential of submerged aquatic vegetation (SAV).

2.2. Field observations and laboratory experiments

Field observations were conducted on July 23 and August 8, 2018, providing the primary dataset used for model calibration, carbon budget analysis, and quantitative evaluation of the contributions from river inflow, tidal exchange, eelgrass metabolism, bottom dilution, and air–water CO_2 flux. In addition, supplementary field observations were conducted in August 2013 and July 2019 solely to provide (i) a reproducibility test of the endmember DIC and TA values and (ii) an inter-annual consistency check of the conceptual DIC model. During these supplementary campaigns, DIC and TA were measured in the three major river inflows and at the tidal inlet connecting Komuke Lagoon to the Sea of Okhotsk, using the same sampling and analytical protocols described below. Vertical profiles of water temperature, dissolved oxygen (DO), and Chl.a were measured at 1 cm intervals using an AAQ-RINKO profiler (JFE Advantech Co. Ltd.). Water samples were collected from 10 cm below the surface and 5 cm above the bottom sediment using a Van Dorn water sampler (Miyamoto Riken Ind. Co.). Mercuric chloride (250 μL) was added to each 250 mL water sample to fix DIC and total alkalinity (TA). DIC and TA were measured using an ATT-15 titration analyzer (Kimoto Electric Co. Ltd.) with a precision of approximately 5 μmol L^{-1}.

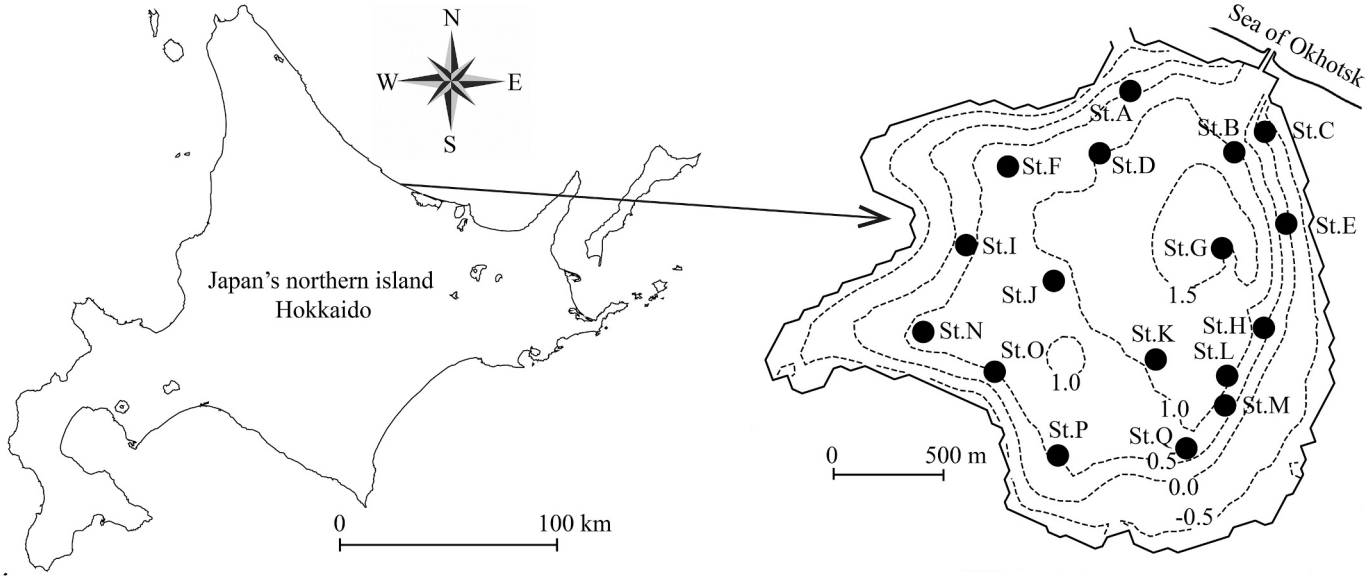


Fig. 1. Bathymetry of Komuke Lagoon. Circles show the water sampling stations.

Laboratory experiments to evaluate photosynthesis were conducted using lagoon water and eelgrass collected on June 25–26, 2018 (Nakayama et al., 2020), and September 15–16, 2023 (Maruyama et al., 2024), from the sampling point (44° 15′ 7.3″ N, 143° 30′ 38.9″ E) shown in Fig. 1. The experiments were conducted outdoors in fine weather using a transparent acrylic tank (150 cm deep, 20 cm wide, and 20 cm long; Fig. 2). Four eelgrass shoots collected from the lagoon were deployed in the tank at 10 cm intervals in water with a salinity of approximately 20 psu. The eelgrass roots were covered with vinyl sheets to prevent oxygen consumption by the roots themselves and by oxygen-demanding substances in the attached sediment. Thermometers (JFE Advantech Co. Ltd., INFINITY-CT) and quantum loggers (JFE Advantech Co. Ltd., DEFI2-L) were deployed in the tank to record data every ten minutes. The experiment began at night, when photosynthesis is inactive, and continued for 24 h. The water was well mixed using a peristaltic pump at a flow rate of 7 mL min^{-1} through a silicon tube (2 mm diameter); water was gently drawn from an inlet at the top and discharged from an outlet at the tank bottom. Approximately 200 mL of water was sampled from the tank, and DIC and TA were measured using a Total Alkalinity meter (Kimoto Electric Co. Ltd., ATT-15) within 2 h of sampling. Additionally, a control experiment was conducted under the same conditions but without eelgrass. Concentrations of NO_3-N, NO_2-N, NH_4-N, and PO_4-P were measured for each experiment using an auto-analyzer (BLTEC Co. Ltd., QuAAtro 2HR). The results of the laboratory experiment conducted on June 25, 2018, were presented in Nakayama et al. (2020); this study proposes a corrected DIC equation by incorporating data from the experiments conducted on September 15–16, 2023 (Maruyama et al., 2024).

2.3. DIC equation

We applied the DIC equation (Eq. 1) to model Net Ecosystem Production (NEP) by eelgrass, incorporating photon flux density and water temperature. This approach differs from that of Nakayama et al. (2020), who used the Arrhenius equation for both respiration and photosynthesis (Eq. 2). In this study, a Jassby-type equation combined with a temperature limitation term was applied to simulate photosynthesis as a function of photon flux density and water temperature (Prokopkin et al., 2006; Hellweger et al., 2008; Staehr and Borum, 2011; Beca-Carretero et al., 2018; Burkholz et al., 2019; Ranjbar et al., 2024). Here, NEPR and NEPP denote the components of NEP attributed to eelgrass respiration and photosynthesis, respectively.

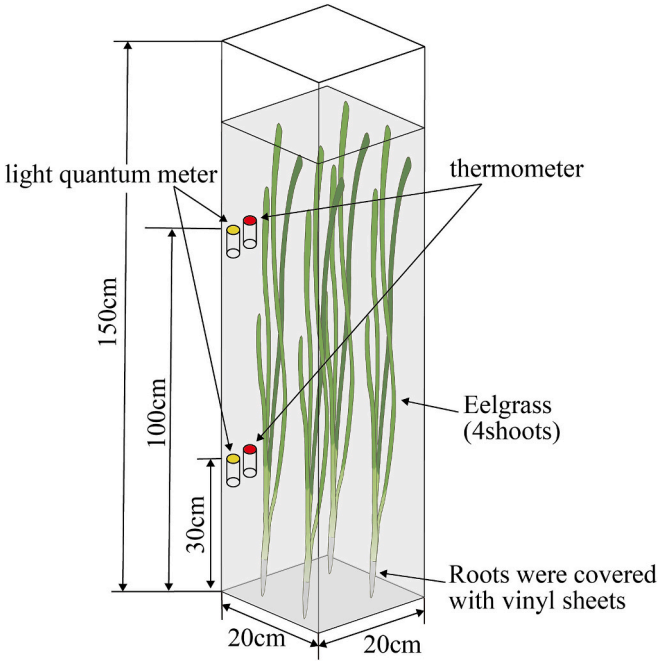


Fig. 2. Outdoor laboratory experiments to measure DIC, water temperature, photon flux density, TA, and nutrients.

$$\frac{d}{dt}(DIC) = \Delta DIC = R_A exp\left(-\frac{E_{aR}}{T_w R}\right) - P_\psi tanh\left(\frac{\alpha_\psi I}{P_\psi}\right) exp\left[-\left(\frac{T_w - T_0}{q}\right)^2\right] = -NEP = NEPR - NEPP \quad (1)$$

$$\frac{d}{dt}(DIC) = \Delta DIC = R_A exp\left(-\frac{E_{aR}}{T_w R}\right) - P_\psi tanh\left(\frac{\alpha_\psi I}{P_\psi}\right) R_P exp\left(-\frac{E_{aP}}{T_w R}\right) = -NEP = NEPR - NEPP \quad (2)$$

where, DIC (μ mol kg^{-1}) is the dissolved inorganic carbon, R_A (μ mol kg^{-1} h^{-1}) is the parameter for respiration, E_{aR} (m^2 kg s^{-2}) is the activation energy for respiration, T_w (K) is the water temperature, R (m^2 kg s^{-2} K^{-1}) is the Boltzmann constant (1.380649×10^{-23}), P_ψ (μ mol kg^{-1} h^{-1}) and α_ψ (m^2 s kg^{-1} h^{-1}) are the parameters for photosynthesis, I (μ mol m^{-2} s^{-1}) is the photon flux density, R_P (−) is the parameter for photosynthesis, T_o (K) is the optimum temperature, and q (K) is the thermal dispersion.

2.4. Net ecosystem production (NEP) model

We performed a detailed hourly analysis of carbon uptake by eelgrass (*Zostera marina*) in Komuke Lagoon to clarify the breakdown of carbon fluxes, including riverine inflow, exchange with the ocean and atmosphere, and bottom dilution. Based on Nakayama et al. (2010) and Nakayama et al. (2020), we treated Komuke Lagoon as a single box and assumed that the volume, DIC, and TA within the box change due to inflows from the three major rivers and tidal exchange (Eqs. 3 to 5). The gas transfer velocity k was computed using AMeDAS 10-m wind. The CO_2 flux (Flux) is defined as positive for outgassing (water → atmosphere) and negative for uptake (atmosphere → water). Thus, in Eq. (3), the term 'Flux' represents a positive DIC supply to the lagoon when atmospheric CO_2 is absorbed. Atmospheric pCO_2 was set to 410 μatm based on the 2018 annual mean observations by the Japan Meteorological Agency. This single-box approach is justified by (i) the absence of vertical stratification confirmed by field observations (see Section 3.1), (ii) the fact that the internal spatial variability of DIC is significantly smaller than the difference between the oceanic and riverine endmembers, making the endmember mixing the primary driver of the lagoon-integrated carbon budget, and (iii) the near-vertically-uniform DIC distribution observed on August 8, 2018 (surface 1680 μmol kg^{-1}, bottom 1660 μmol kg^{-1}), which confirms well-mixed conditions at the whole-lagoon scale.

In addition to these empirical justifications, the single-box framework was deliberately preferred over a three-dimensional hydrodynamic–biogeochemical model for two reasons. First, a three-dimensional simulation would require spatially resolved forcing that exceeds the available observational constraints, including high-resolution bathymetry (<10 m), three-dimensional current fields, spatially distributed benthic organic matter content, and site-specific porewater DIC profiles; such data are not presently available for Komuke Lagoon. Second, the scientific objective of this study is to quantify the lagoon-integrated carbon budget — in particular the relative contributions of riverine inflow, tidal exchange, bottom dilution, atmospheric exchange, and eelgrass NEP — rather than to resolve internal spatial structure. For this lagoon-scale accounting, a well-constrained box model provides superior traceability and transparency of each source and sink term, while a three-dimensional model would introduce additional parameter uncertainty that is unwarranted given

the observational base. Spatially explicit processes not captured by this approximation (e.g., localized outgassing near river mouths, heterogeneity in bottom dilution) are discussed as limitations in Section 4.4.

A key feature of the model used in this study is the inclusion of CO_2 exchange flux across the air-water interface, which was not considered in Nakayama et al. (2020) (Fig. 3). Furthermore, this model is characterized by the incorporation of TA, a parameter often neglected when processes such as calcification are absent.

$$\frac{d}{dt}\left(V \times DIC_{lagoon}\right) = q_{river} \times DIC_{river} + q_{tide} \times \begin{cases} DIC_{ocean} & q_{tide} > 0 \\ DIC & q_{tide} < 0 \end{cases} - NEP \times V_{SAV} + B - Flux \times A_{lagoon} - q_{river} \times DIC \tag{3}$$

$$\frac{d}{dt}\left(V \times TA_{lagoon}\right) = q_{river} \times TA_{river} + q_{tide} \times \begin{cases} TA_{ocean} & q_{tide} > 0 \\ TA & q_{tide} < 0 \end{cases} \tag{4}$$

$$\Delta VAR^{n}_{lagoon} = \frac{\frac{d}{dt}\left(V \times VAR_{lagoon}\right)}{V^{n+1}_{lagoon}} + \left(\frac{V^{n}_{lagoon}}{V^{n+1}_{lagoon}} - 1\right) \bullet VAR^{n}_{lagoon} \tag{5}$$

where, V is the lagoon volume (m^3), DIC_{lagoon} is DIC in Komuke Lagoon (μmol kg^{-1} h^{-1}) , q_{river} is the inflow discharge (m^3 h^{-1}), DIC_{river} is DIC of the inflow (μmolkg^{-1} h^{-1}), q_{tide} is the tidal flux (positive corresponds to the flood tide) (m^3 h^{-1}), DIC_{ocean} is DIC of the Okhotsk Sea (μmol kg^{-1} h^{-1}), NEP is NEP of eelgrass (μmol kg^{-1} h^{-1}), V_{SAV} is the volume of eelgrass (m^3), B is the dilution from the lagoon bottom (m^3 μmol kg^{-1} h^{-1}), $Flux$ is the CO_2 between the water surface and the atmosphere (m μmol kg^{-1} h^{-1}), A_{lagoon} is the water surface area of Komuke Lagoon ($= 3.8 \times 10^6$) (m^2), TA_{lagoon} is TA in Komuke Lagoon (μmol kg^{-1} h^{-1}), TA_{ocean} is TA of the Okhotsk Sea (μmol kg^{-1} h^{-1}), ΔVAR^{n}_{lagoon} is the change in DIC or TA from time step n and n + 1 (μmol kg^{-1}), VAR^{n}_{lagoon} is DIC or TA (μmol kg^{-1}), V^{n+1}_{lagoon} is the lagoon volume at time step n + 1 (m^3), V^{n}_{lagoon} is the lagoon volume at time step n (m^3).

The seasonal growth cycle of eelgrass in Komuke Lagoon was prescribed as follows. Because shoot density and leaf length are strongly correlated with the standing crop, the temporal change in standing crop was used as a proxy for eelgrass growth. The annual water-temperature cycle in Komuke Lagoon is close to that in Notsuke Bay (eastern Hokkaido), where Mizushima (1985) reported the monthly variation of the eelgrass standing crop. Given this similarity in thermal forcing, the annual growth cycle of *Zostera marina* in the two lagoons is assumed to be comparable. The monthly standing crop reported by Mizushima (1985) was therefore normalized by its July–August maximum and used to prescribe the annual growth curve in Komuke Lagoon (40% of the maximum in December–May, 100% in July–September, with linear interpolation in transition months).

The dilution from the lagoon bottom B was prescribed following Nagatomo et al. (2023) and Nakayama et al. (2020), who developed a Spatially integrated DIC (SiDIC) model for Komuke Lagoon and derived a site-specific bottom dilution rate that is consistent with the independent DIC mass-balance estimate of Nakayama et al. (2020). Specifically, we adopted, $B = B_0 A_{lagoon}$, where $B_o = 355$ mg-CO_2 m^{-2} d^{-1} represents the lagoon-averaged bottom dilution and $A_{lagoon} = 3.8 \times 10^6$ m^2. This value integrates (i) aerobic and anaerobic mineralization of sedimentary organic carbon, and (ii) advective/diffusive transport of porewater DIC across the sediment–water interface. For simplicity, B is treated as time-invariant, which is consistent with the steady-state assumption of the underlying SiDIC framework. The uncertainty of B and its propagation to the simulated lagoon DIC and the summer-validated, annually-projected carbon budget are examined through sensitivity simulations presented in Section 4.3.

The initial values were set to 3,333,000 m^3 for V_{lake} and 2000 μmol kg^{-1} for DIC_{lagoon}. The riverine and oceanic DIC endmembers for the 2018 carbon-budget simulation were determined from the July and August 2018 campaigns, and their temporal stability was subsequently confirmed by comparison with the supplementary observations in August 2013 and July 2019 (reproducibility check). Accordingly, DIC_river and DIC_ocean were set to 540 μmol kg^{-1} (standard deviation across the three-year dataset: 110 μmol kg^{-1}) and 1980 μmol kg^{-1} (standard deviation: 20 μmol kg^{-1}), respectively. The small variability in DIC_{ocean} (~1% of the mean) reflects the strong buffering capacity of the Sea of Okhotsk, supporting the use of a constant oceanic endmember. Although DIC_{river} exhibited larger relative variability (~20%), this deviation is small compared to the endmember contrast ($DIC_{ocean} - DIC_{river} \approx 1440$ μmol $kg^{-1} \approx 8\%$ of the contrast), indicating that the constant-endmember formulation is appropriate for evaluating the lagoon-integrated carbon budget. The sensitivity of the results to the ±1 σ range of DIC_{river} is discussed in Section 4.3.

Riverine inflow was estimated using a storage function validated by field observations. The exchange flow rate with the ocean was determined using a function based on the water level difference between Komuke Lagoon and the Sea of Okhotsk, which was derived from a three-dimensional numerical simulation (Fig. 4a and b). Regarding eelgrass abundance, based on field observations, the biomass was set to 40% from December to May and 100% from July to September. Values for the transition periods (May–July and September–December) were linearly interpolated. The shoot density of eelgrass was assumed to be 250 shoots m^{-2}. Meteorological data, including solar radiation, wind speed, air temperature, precipitation, and atmospheric pressure, were obtained from the Automated Meteorological Data Acquisition System (AMeDAS). These seasonal biomass fractions are based on field biomass

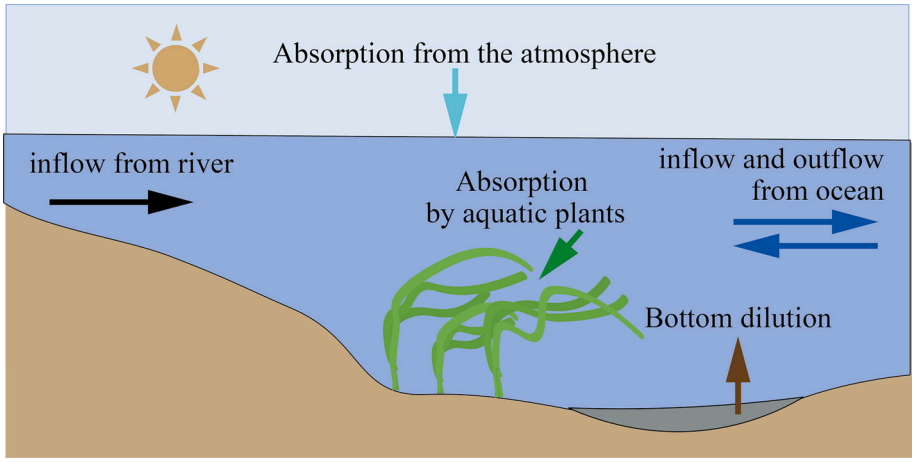


Fig. 3. A conceptual DIC model for Komuke Lagoon.

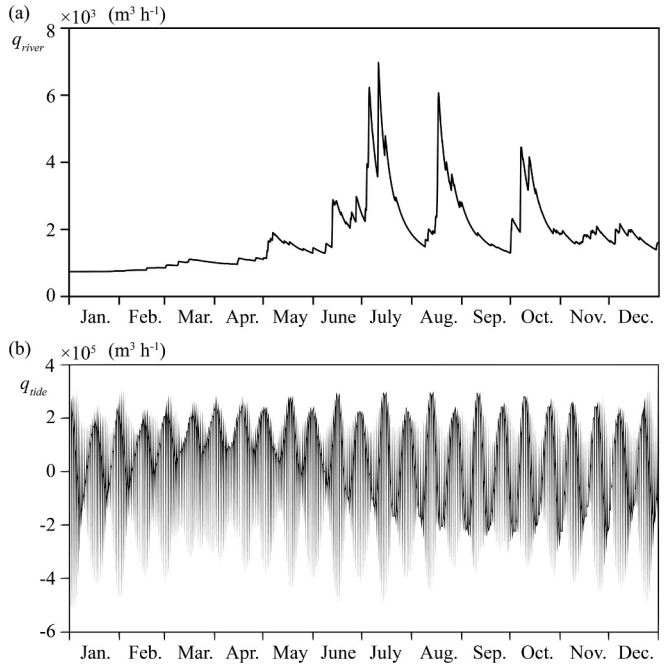


Fig. 4. River and tidal inputs. (a) River inflow from January to December 2018. Discharge was estimated using a storage function model based on the field observations. (b) Seawater exchange flux between Komuke Lagoon and the Okhotsk Sea from January to December 2018. Seawater exchange flux was modeled by the water level difference between Komuke Lagoon and the Okhotsk Sea based on the field observations and three-dimensional hydrological simulations.

surveys of eelgrass distribution conducted in Komuke Lagoon (Watanabe and Kuwae, 2021), and are consistent with the known phenological cycle of *Zostera marina* in temperate Hokkaido, where low irradiance and low water temperatures during winter substantially reduce growth and biomass. The shoot density of 250 shoots m^{-2} represents the mean value observed during the summer peak growth period at representative stations (Maruyama et al., 2024). To evaluate the sensitivity of the NEP estimates to uncertainty in these biomass parameters, a sensitivity simulation for 2018 was performed by varying the seasonal biomass fraction by 20%. Because NEP scales linearly with the prescribed biomass, this produced a proportional (20%) change in the annually-integrated NEP projection, while the relative contributions of tidal exchange, river inflow, bottom dilution, and air–water CO_2 flux remained unchanged. This confirms that the ranking of carbon sources and sinks in Table 2 is robust to reasonable uncertainties in eelgrass coverage.

3. Results

3.1. Field observations

In Komuke Lagoon, salinity levels remain close to those of seawater because the tidal exchange flux significantly exceeds river discharge. Furthermore, the lagoon connects to the Sea of Okhotsk via a 15 m wide channel, where tidal currents can exceed 2 m s^{-1}. This strong flow ensures that intruding oceanic water is well-mixed, thereby suppressing the formation of stratification. Consequently, field observations conducted on July 23 and August 8, 2018, revealed uniform vertical profiles for water temperature and salinity across all sampling sites (Fig. 5), indicating that no distinct stratification was present. While Lin et al. (2023) demonstrate that a two-layer box model is required when stratification is evident, the observed lack of stratification in this study supports the validity of a single-box model approach.

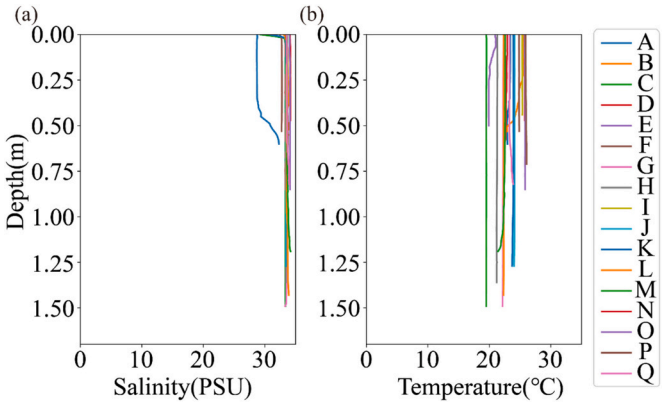


Fig. 5. Vertical profiles of (a) salinity and (b) water temperature at all 17 sampling stations on August 8, 2018.

Regarding DIC, the mean concentrations near the water surface and the bottom layer on July 23, 2018, were 1680 μmol kg^{-1} and 1790 μmol kg^{-1}, respectively. The higher DIC observed in the bottom layer compared to the surface is attributed to the presence of slight stratification, which likely caused flow stagnation and trapped the benthic release within the eelgrass bed. On August 8, the mean DIC concentrations near the surface and bottom were 1680 μmol kg^{-1} and 1660 μmol kg^{-1}, respectively, indicating a nearly vertically uniform distribution. The spatial deviation of DIC across 17 sites (surface and bottom) was 200 μmol kg^{-1} on July 23, 2018, and 230 μmol kg^{-1} on August 8, exhibiting a trend of lower values near the river mouth and higher values near the Sea of Okhotsk. The supplementary field observations conducted in August 2013 and July 2019 yielded endmember values that were consistent with the 2018 campaigns, serving as a reproducibility check and a confirmation of the inter-annual stability of the endmembers. Across the three-year dataset, river-water DIC averaged 540 ± 110 μmol kg^{-1} and oceanic DIC averaged 1980 ± 20 μmol kg^{-1}. This result justifies the use of the 2018-based, constant endmembers in the carbon-budget simulation discussed in Section 4. However, this spatial gradient primarily reflects the mixing continuum between the freshwater (river-mouth) and oceanic (tidal-inlet) endmembers, both of which are explicitly represented in the box model as source terms ($q_{river} \times DIC_{river}$ and $q_{tide} \times DIC_{ocean}$). The observed internal DIC variability (200–230 μmol kg^{-1}) is relatively small compared to the large gradient between the riverine and oceanic endmembers (~1440 μmol kg^{-1}). Therefore, the observed horizontal DIC variability is implicitly incorporated through the endmember mixing formulation, rather than treated as unresolved internal heterogeneity. The eelgrass meadow, which dominates the NEP term, occupies a spatially extensive area where DIC values are close to the lagoon mean, supporting the use of lagoon-averaged DIC for evaluating the eelgrass contribution to the carbon budget.

3.2. Coefficients for the DIC equation

Nakayama et al. (2020) determined the parameters for the eelgrass DIC equation using results from laboratory experiments conducted in 2018. In this study, we refined the coefficients of the eelgrass DIC equation by incorporating additional laboratory experiments conducted in 2023 (Maruyama et al., 2024). The 2023 experiments exhibited a trend similar to that of 2018, with DIC decreasing during the day and increasing at night (Fig. 6a). However, at 10:00 pm on September 15, 2023, the DIC value was notably lower than adjacent values. Additionally, water temperatures in the 2023 laboratory experiment exceeded 30 °C between 12:00 and 19:00 on September 15 (Fig. 6b). Since observed water temperatures in Komuke Lagoon do not exceed 30 °C even in summer, these data points were regarded as outliers and were

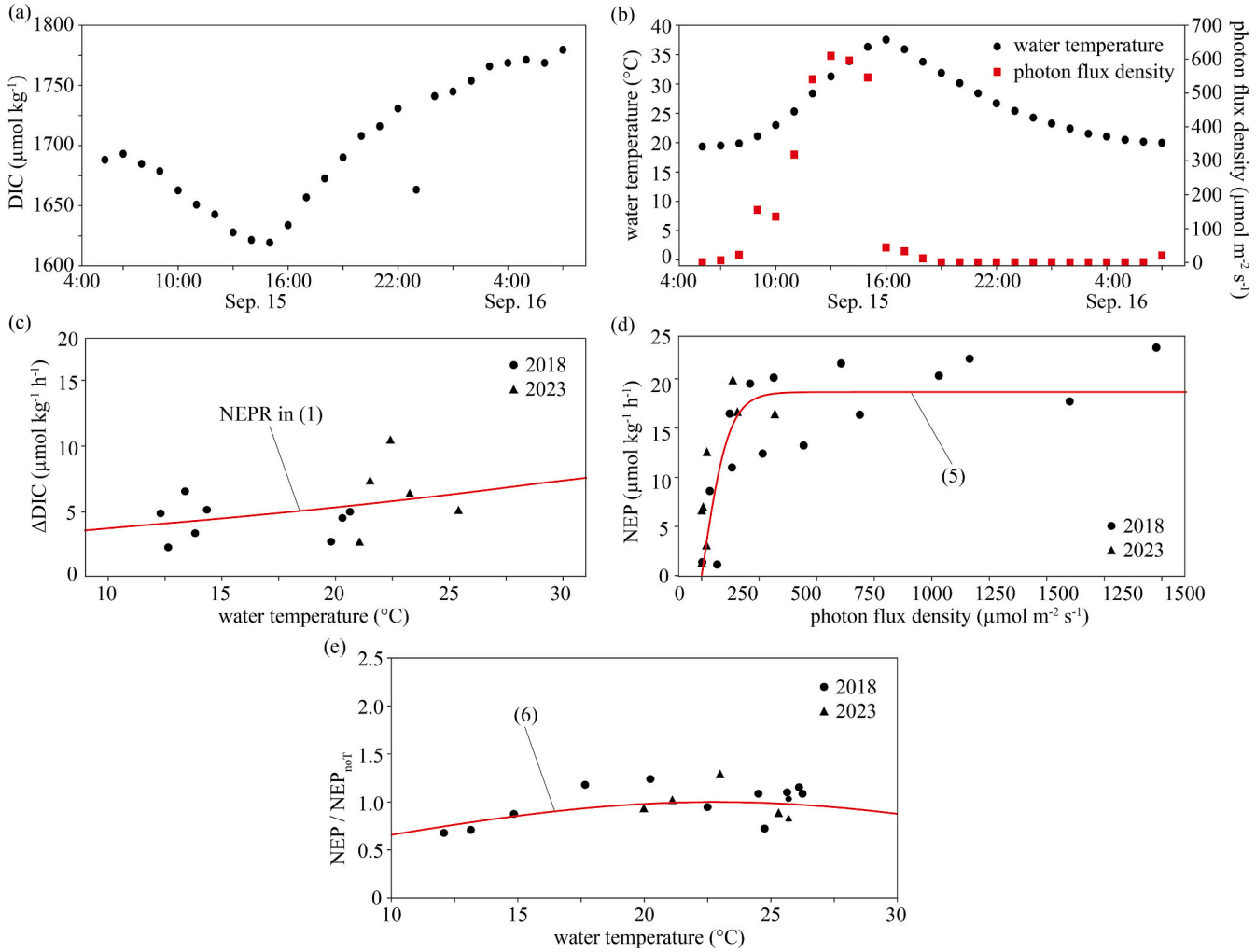


Fig. 6. Laboratory experiments for the DIC equation in September of 2023. (a) DIC, (b) Water temperature and photon flux density, (c) Water temperature vs. ΔDIC, (d) Photon flux density vs. NEPP, and (e) Water temperature vs. NEPP / $NEPP_{noT}$.

excluded from the analysis for parameter estimation.

Following Nakayama et al. (2020), parameter estimation was performed by first focusing on the nighttime period to determine the coefficients associated with respiration (NEPR) (Table 1 and Fig. 6c). Here, ΔDIC represents the rate of change in DIC per hour. Using the least squares method, the estimated values were $R_A = 1.03 \times 10^5$ and $E_{aR} = 3.99 \times 10^{-20}$. In Nakayama et al. (2020), delta DIC increased by more than a factor of three as the water temperature rose from 20 °C to 30 °C; however, with the parameters obtained in this study, the increase is less than a factor of 1.5. This difference is likely attributed to the fact that experiments were conducted in different seasons—not only in June 2018 but also in September 2023—which allowed for the consideration of conditions with higher water temperatures.

With the values of R_A and E_{aR} determined, the carbon emissions due to respiration (NEPP) can be calculated. Regarding NEPP, the component related solely to photon flux density is defined as $NEPP_{noT}$, and P_Ψ and α_Ψ are estimated.

$$NEPP_{noT} = P_\Psi tanhtanh\left(\frac{\alpha_\Psi I}{P_\Psi}\right) \tag{6}$$

Using the least squares method, the estimation yielded $P_\Psi = 18.7$ and $\alpha_\Psi = \frac{18.7}{116}$ (Fig. 6d). A photon flux density of 116 μmol m^{-2} s^{-1} or higher implies that photosynthesis is occurring at its maximum rate. Since this level is reached three hours after sunrise, it is inferred that photosynthesis is performed at maximum capacity for the majority of the daylight hours. The change in parameter values is likely attributed to the addition of data from September 2023, which increased the number of data points for low photon flux density conditions. Finally, the parameters for the water temperature component of NEPP were estimated using Eq. (7).

$$exp\left[-\left(\frac{T - T_0}{q}\right)^2\right] = \frac{NEPP}{NEPP_{noT}} \tag{7}$$

Using the least squares method, the estimation yielded $T_0 = 22.8$ and $q = 19.7$ (Fig. 6e). It was shown that, similar to carbon emissions from respiration, carbon uptake due to photosynthesis might not be significantly affected by water temperature. This is considered to be due to the fact that the ratio $\frac{NEPP}{NEPP_{noT}}$ showed a decreasing trend, particularly when the water temperature was 22.9 °C or higher.

Table 1
Parameters for the DIC equation.

Nakayama et al. (2020)		This study	
R_a	1.04×10^{17}	R_a	1.03×10^5
E_{aR}	1.52×10^{-19}	E_{aR}	3.99×10^{-20}
P_Ψ	21.5	P_Ψ	18.7
α_Ψ	21.5/200	α_Ψ	18.7/116
R_P	2.30×10^7	T_0	22.8
E_{aP}	6.90×10^{-20}	q	19.7

3.3. NEP model

In the conceptual DIC model, the DIC concentrations of river water and seawater were set to 540 ± 110 μmol kg^{-1} and 1980 ± 20 μmol kg^{-1}, respectively. The observational results obtained on July 23 and August 8 showed mean DIC values of 1736 μmol kg^{-1} and 1671 μmol kg^{-1}, respectively. The observations were conducted between 10:00–17:00 and 11:00–17:00, respectively. It was verified that the conceptual DIC model successfully reproduced the in situ observational results (Fig. 7c). The model goodness-of-fit was evaluated by computing the root mean square error (RMSE) between the simulated DIC and the lagoon-averaged observed DIC for each observation campaign. The RMSE was 35 μmol kg^{-1} for July 23, 2018 and 28 μmol kg^{-1} for August 8, 2018. Both values are smaller than the spatial standard deviation of DIC across the 17 sampling stations (200–230 μmol kg^{-1}), which is shown as ±1 SD vertical error bars on the observed data points in Fig. 7c, confirming that the conceptual DIC model reproduces the lagoon-averaged DIC within the spatial variability of the observations. It was found that DIC values in Komuke Lagoon decreased from January to June, reached a minimum in July, and increased thereafter. This suggests that NEP increased from January to June, and subsequently, as NEP values decreased, the DIC values in the lake increased. Significant fluctuations in DIC were observed in early July, late August, and mid-October. These rapid decreases in DIC were attributed to the large inflow of river water during these periods.

To examine the effect of NEP, a numerical simulation was conducted assuming the absence of eelgrass, i.e., by setting NEP to zero (Fig. 7d). Compared to the case with eelgrass, the results without eelgrass showed higher DIC values throughout the year and a smaller range of fluctuation, demonstrating the significant effect of NEP. By setting NEP to zero, the fluctuations in DIC in early July, late August, and mid-October became more distinct, revealing that river water inflow contributes significantly to the decrease in DIC.

To test the reproducibility of the conceptual DIC model and to examine whether its skill is stable across years, the same model was additionally applied to 2013 and 2019 using the meteorological, hydrological, and tidal forcing of each respective year. The simulated DIC values were compared with the supplementary field observations in August 2013 and July 2019 (Fig. 7). The model reproduced the observed lagoon-averaged DIC within the observational uncertainty in both years (error = 55 μmol kg^{-1} in 2013 and 98 μmol kg^{-1} in 2019), which is comparable to the mean error obtained for 2018 (63 μmol kg^{-1}). The simulated full annual DIC cycle in 2013 and 2019 followed the same seasonal pattern as that in 2018 — DIC decreasing from January through late spring as NEP increased, reaching a minimum in July, and gradually recovering in autumn and winter as NEP declined. These results demonstrate that (i) the calibrated DIC equation and the conceptual DIC model are reproducible when applied to independent years, and (ii) no substantial inter-annual drift exists in the model skill under the meteorological and hydrological conditions encountered in Komuke Lagoon. Because the detailed quantitative partitioning of the summer-validated carbon budget (integrated over the simulated calendar year) requires simultaneous and densely sampled field data for DIC, TA, salinity, riverine endmembers, and laboratory-derived photosynthesis parameters, the contribution analyses presented in Sections 4.2 and 4.3 were restricted to 2018, for which such a dataset is fully available.

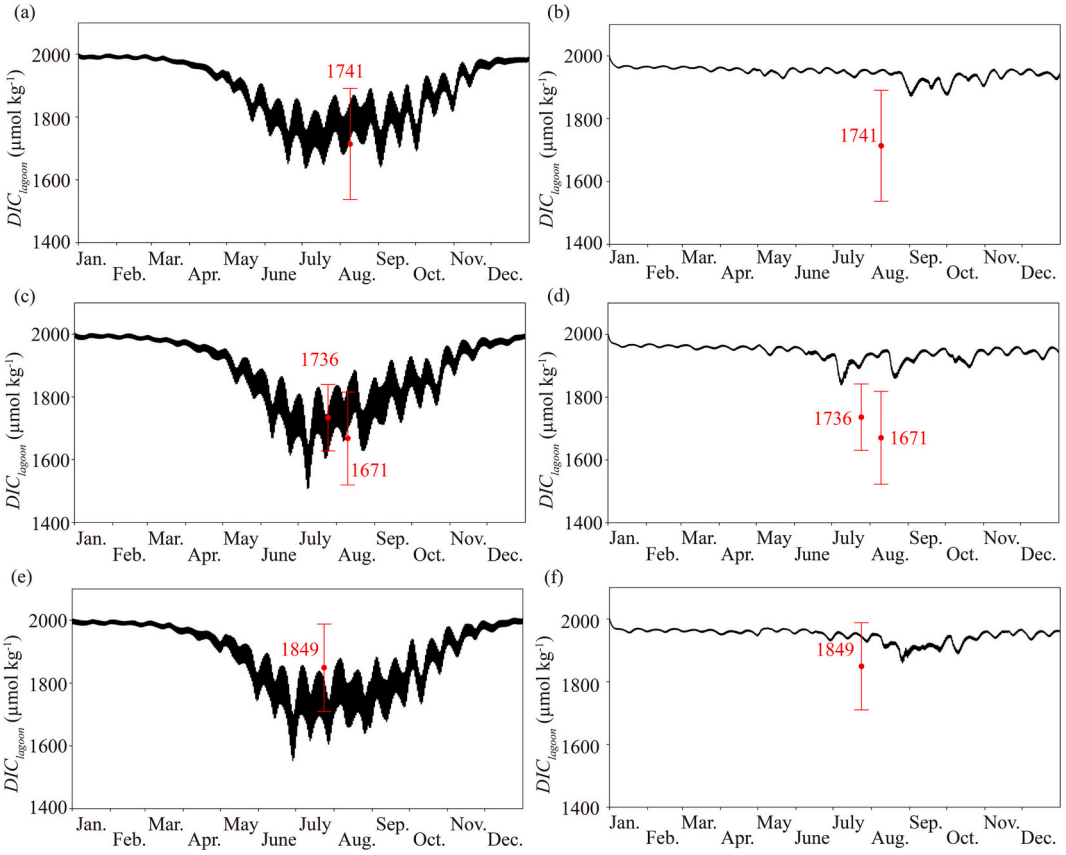


Fig. 7. DIC simulated by the conceptual DIC model. (a), (c), (e) Comparisons with the field observations. Panel (c) shows the 2018 simulation used for calibration and for the quantitative carbon-budget analysis, while panels (a) and (e) show the 2013 and 2019 simulations performed as a reproducibility test and an inter-annual consistency check, respectively. Red circles indicate the mean DIC (a) in August 2013, (c) on July 23 and August 8, 2018, and (e) in July 2019. Vertical error bars represent ±1 standard deviation of DIC across the 17 sampling stations (surface and bottom layers). The error between the simulated and observed lagoon-averaged DIC was 55 μmol kg^{-1} in 2013 and 98 μmol kg^{-1} in 2019, which is comparable to the mean error obtained for 2018 (63 μmol kg^{-1}). (b), (d), (f) Simulated DIC for 2013, 2018, and 2019, excluding NEP, is shown to illustrate the influence of eelgrass metabolism.

4. Discussion

4.1. Effect of water temperature and photon flux density on DIC

The traditional Arrhenius equation, while effective for simple chemical reactions, often fails to represent the complex physiological responses of whole organisms like *Zostera marina* across a wide temperature range. Lee et al. (2007) emphasized that seagrasses possess species-specific optimum temperatures, beyond which metabolic efficiency inevitably declines. In our study, the inclusion of a temperature limitation term—following the modeling framework for aquatic organisms proposed by Ranjbar et al. (2024)—allows for the reproduction of this characteristic thermal inhibition. By incorporating an optimum temperature and thermal dispersion, the refined DIC equation more accurately reflects the biological reality that excessive warming suppresses net ecosystem production (NEP). This transition from an exponential Arrhenius model to an optimum-based model is essential for high-precision carbon budget evaluations in temperate lagoons where summer temperatures may approach or exceed the physiological limits of eelgrass. The Arrhenius formulation assumes monotonic temperature dependence and is strictly valid only within a narrow range below the thermal optimum. For biological processes such as photosynthesis, a bell-shaped response with an optimum temperature T_o is well documented (Lee et al., 2007), reflecting (i) the thermal instability of the oxygen-evolving complex of photosystem II, (ii) reduced CO_2 specificity of Rubisco at high temperatures, and (iii) enhanced photorespiration. Accordingly, the Gaussian temperature-limitation term $\exp.[-((T - T_o)/q)^2]$ adopted here (Eq. 1) is physiologically more realistic than the Arrhenius formulation for lagoon temperatures that exceed 22.8 °C in summer.

Generally, as summarized by Lee et al. (2007), the optimal temperatures for seagrass growth and photosynthesis are often higher for tropical/subtropical species than for temperate species. For *Zostera marina*, optimal temperatures are reported to be between 15 °C and 20 °C (e.g., Moore et al., 1996; Lee et al., 2006; Watanabe et al., 2005). Field observations have also shown that while they grow significantly in spring and autumn, they decrease in summer, partly due to overcrowding (Dennison et al., 1987; Lee et al., 2005). Based on these findings, since *Zostera marina* has optimal temperatures, applying the Arrhenius equation, which assumes that photosynthetic efficiency increases as water temperature rises, is considered inappropriate. The results of this study, which incorporated new experimental data, showed that photosynthetic efficiency decreased with rising water temperatures. Therefore, it is suggested that future studies should apply optimal temperatures to the DIC equation (Fig. 6e).

The decline of photosynthetic efficiency above the thermal optimum is not a feature unique to *Zostera marina* in Komuke Lagoon but is a common physiological trait of temperate *Zostera* species more broadly. The comprehensive review of seagrass physiology by Lee et al. (2007) demonstrates that temperate congeners such as *Zostera japonica*, *Zostera noltii*, and *Zostera caespitosa* all exhibit a bell-shaped photosynthetic response to water temperature, with species-specific thermal optima beyond which net photosynthesis declines due to enzymatic inhibition, elevated photorespiration, and increased dark respiration. Reported optima range from approximately 15–25 °C for *Z. marina* and are shifted slightly upward (approximately 20–30 °C) for *Z. japonica*, consistent with its distribution in shallower and warmer intertidal habitats. The thermal optimum obtained in this study ($T_o = 22.8$ °C) falls within the upper range reported for *Z. marina* populations, providing additional support for the physiological plausibility of the calibrated parameters. Furthermore, the Jassby-type formulation combined with the Gaussian-shaped temperature limitation term (Eqs. 6 and 7) does not rely on parameters that are specific to a single species; T_o and q are species- and site-specific coefficients that can be recalibrated for any temperate seagrass exhibiting a bell-shaped thermal response. The present NEP formulation is therefore transferable to other temperate *Zostera* species and, more broadly, to blue carbon assessments in temperate seagrass-dominated lagoons, where neglect of the high-temperature decline in photosynthesis would otherwise lead to a systematic overestimation of NEP during summer.

In this study, the photon flux density at which photosynthetic efficiency saturates was shown to be 116 μmol m^{-2} s^{-1}. Cabello-Pasini et al. (2003) indicated a range of 10 μmol m^{-2} s^{-1} to 350 μmol m^{-2} s^{-1}, while Touchette (1999) showed that it can reach 450 μmol m^{-2} s^{-1}. Herzka and Dunton (1998) demonstrated that the photon flux density for saturation of photosynthetic efficiency is lowest in winter, increases toward spring, and peaks in summer. In the present study, the data were obtained in early summer 2018 and autumn 2023; the photon flux density at which photosynthetic efficiency saturated was higher in 2018 than in 2023. Given this point, it is considered necessary in future research to vary the value of the saturating photon flux density using seasonal average water temperatures. The physiological basis for this seasonal difference involves two interrelated mechanisms. Under high ambient irradiance in summer, *Zostera marina* downregulates its light-harvesting efficiency by reducing chlorophyll *a* content and reorganising thylakoid membrane composition, while simultaneously upregulating carbon-fixation capacity through increased Rubisco enzyme content and activity (Staehr and Borum, 2011). These complementary adjustments collectively raise the irradiance required to saturate photosynthesis in summer. The reverse acclimation occurs in autumn and winter, consistent with the lower saturation irradiance observed in the September 2023 experiments. Analogous seasonal photoacclimation has been documented for *Zostera marina* by Olesen and Sand-Jensen (1993), who showed that both the maximum photosynthetic rate and the light saturation point increase from winter to summer in response to rising day length. These findings are also consistent with the seasonal increase of the light saturation point for temperate seagrasses reported by Herzka and Dunton (1998) and support the need for seasonally varying saturation irradiances in long-term carbon budget models.

4.2. Contribution of inflow, seawater exchange, NEP, dilution from the lagoon bottom and surface flux on carbon sequestration

All contribution analyses presented in this section, including Fig. 8 and Table 2, were conducted for the calendar year 2018, for which simultaneous field observations of DIC, TA and salinity and laboratory photosynthesis experiments most densely constrain the model. The 2013 and 2019 simulations described in Section 3.3 were used only for reproducibility and inter-annual consistency checks and are therefore not revisited here. In blue carbon ecosystems, the extent of the influence of river inflow, seawater exchange, absorption by *Zostera marina*, dilution from the lagoon bottom and water surface flux has not been sufficiently examined, and there is a need to clarify their breakdown (Nellemann et al., 2009). The model proposed in this study allows for the separation and consideration of each of these effects. Therefore, a reproduction simulation was conducted by setting the river inflow term to zero, defining the result as DIC_{lagoon} without inflow. The effect of river inflow was examined by calculating (DIC_{lagoon} − DIC_{lagoon} without inflow). Similar calculations were performed for tides, aquatic plants, bottom dilution and flux at the water surface (Fig. 8).

Since the DIC of river water is 540 μmol kg^{-1}, which is lower than the DIC values in Komuke Lagoon, it was found that river water inflow has the effect of decreasing DIC by a maximum of approximately 200 μmol kg^{-1} (Fig. 8a). In contrast, since the DIC of seawater is 1980 μmol kg^{-1}, seawater exchange via tides was found to have the effect of increasing DIC by a maximum of approximately 2000 μmol kg^{-1} (Fig. 8b). The effect of *Zostera marina* decreases DIC by approximately 300 μmol kg^{-1}, demonstrating that it governs the DIC within the lagoon (Fig. 8c). Since the DIC values in Komuke Lagoon are lower than atmospheric values, the water surface flux increased DIC by approximately 30 μmol kg^{-1} (Fig. 8d). This effect is about 2% relative to the absolute value of DIC,

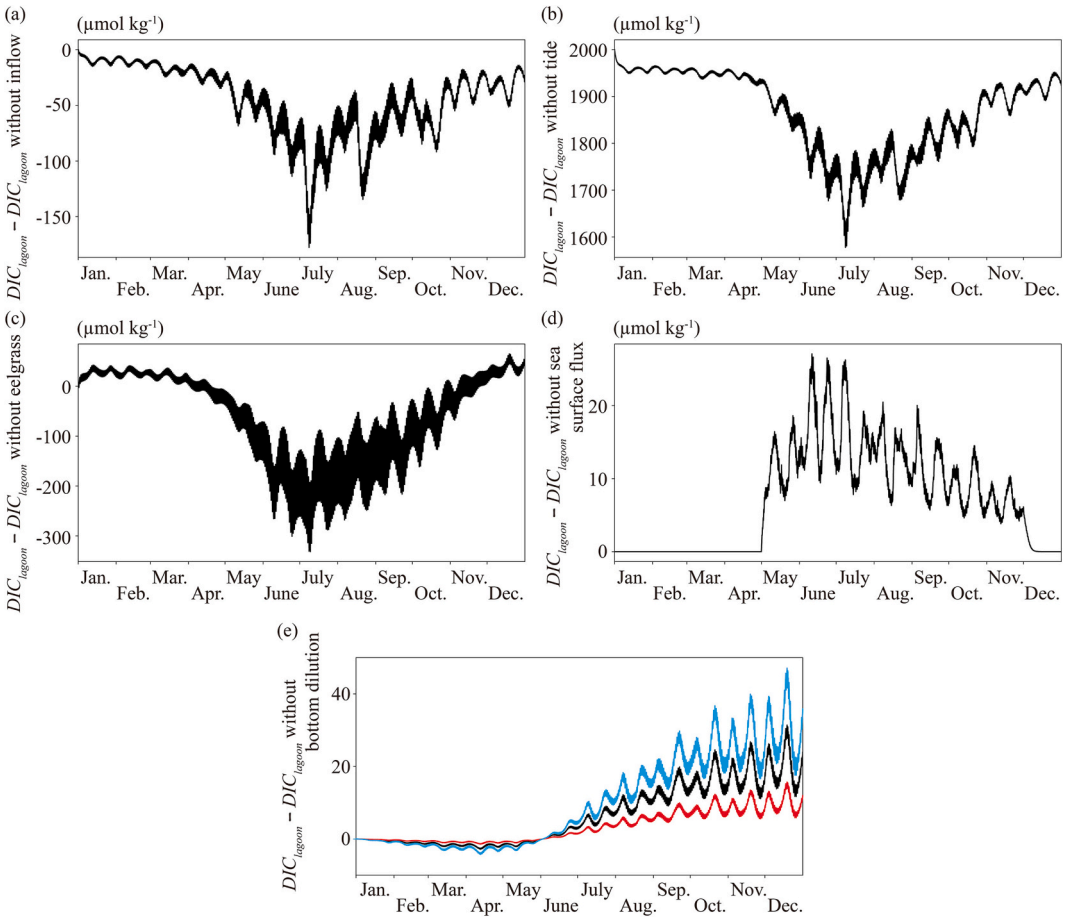


Fig. 8. Contributions of (a) river inflow, (b) seawater exchange, (c) *Zostera marina* net ecosystem production, (d) water surface CO_2 flux, and (e) bottom dilution(B) to the simulated lagoon-averaged DIC. Each contribution is defined as the difference between the baseline simulation and a simulation in which the corresponding source/sink term is set to zero. Blue and red envelopes in (e) indicate the B ± 50% sensitivity range reported in Section 4.3.

Table 2
Based on the 2018 simulation, the carbon flux (summer-validated, integrated over the simulated calendar year) of surface flux, inflow, tide, bottom dilution, carbon sequestration due to *Zostera marina*, and outflow. The flux components shown here are validated against summer (July–August) observations of DIC and TA; the integration over the remaining months is reported as a model projection. Positive and negative values correspond to the increase and decrease in CO_2 in Komuke Lagoon. The total CO_2 uptake driven by tides, river discharge, bottom dilution, and air-water surface flux is normalized to 100%. Consequently, CO_2 absorptions by *Zostera marina* and outflow are presented as a percentage relative to this total. Positive and negative values correspond to the increase and decrease in CO_2 in Komuke Lagoon. For the air-water exchange, *Flux* is reported as a positive value (127 mg-CO_2 m^{-2} d^{-1}), indicating that atmospheric uptake acts as a supply to the lagoon. The sensitivity of each component to ±50% perturbation of the bottom dilution B is reported in Section 4.3.

	Base	DIC_{river} + 110	DIC_{river} − 110	B + 50%	B − 50%	NEP + 20%	NEP − 20%
$-Flux$	127 (5.4%)	124 (5.3%)	130 (5.6%)	122 (5.0%)	131 (5.9%)	141 (5.4%)	110 (5.3%)
$\frac{q_{river} \times DIC_{river}}{A_{lagoon}}$	304 (13.0%)	359 (15.3%)	249 (10.7%)	304 (12.4%)	304 (13.7%)	304 (11.6%)	304 (14.7%)
$\frac{[q_{tide} \times \langle DIC_{ocean}\ q_{tide} > 0\ DIC\ q_{tide} < 0\ ]}{A_{lagoon}}$	1551 (66.4%)	1502 (64.2%)	1601 (68.6%)	1494 (60.9%)	1494 (72.4%)	1739 (66.6%)	1366 (66.1%)
$\frac{B}{A_{lagoon}}$	355 (15.2%)	355 (15.2%)	355 (15.2%)	532 (21.7%)	177 (8.0%)	426 (16.3%)	284 (13.8%)
$-\frac{NEP \times V_{SAV}}{A_{lagoon}}$	− 1183 (− 50.6%)	− 1183 (− 50.6%)	− 1183 (− 50.7%)	− 1183 (− 48.2%)	− 1183 (− 53.3%)	− 1419 (− 54.4%)	− 946 (− 45.8%)
$\frac{-q_{river} \times DIC}{A_{lagoon}}$	− 1154 (− 49.4%)	− 1157 (− 49.4%)	− 1152 (− 49.3%)	− 1269 (− 51.8%)	− 1038 (− 40.7%)	− 1191 (− 45.6%)	− 1118 (− 54.2%)

proving that the assumption in Nakayama et al. (2020) that the water surface flux of DIC can be ignored in the conceptual model was correct. Tokoro et al. (2014) reported direct atmospheric CO_2 uptake by coastal submerged aquatic vegetation in Japan, but those measurements were made in open coastal settings where the diluting effect of large oceanic DIC inputs is less pronounced. Conversely, in tropical restricted-lagoon systems with strong tidal exchange, tidal DIC supply was similarly found to dominate the carbon budget (Nakayama et al., 2022), consistent with our findings. Furthermore, it was found that bottom dilution has the effect of increasing DIC by approximately 30 μmol kg^{-1} (Fig. 8e).

4.3. Flood effect on carbon capture by eelgrass from the aspect of TA

While Total Alkalinity (TA) is typically considered in Dissolved

Inorganic Carbon (DIC) analysis when biochemical changes such as calcification are present, the effects of river inflow are often disregarded (Tokoro et al., 2014). However, Nakayama et al. (2022) conducted an analysis accounting for the difference in TA between river water and the open ocean, demonstrating that this influence cannot be ignored. Changes in TA result in variations in pCO_2, thereby affecting the CO_2 flux at the water surface. Consistent with Section 4.2, the TA-related analysis presented here focuses exclusively on 2018, the target year of the carbon-budget evaluation, during which several flooding events occurred (Fig. 4a). We therefore examined the extent to which river-water inflow affected pCO_2 in 2018 (Fig. 9). TA varied between approximately 2000 μmol kg^{-1} and 2150 μmol kg^{-1}, indicating that assuming a constant TA value for Komuke Lagoon is problematic (Fig. 9a). Analyses assuming a constant TA resulted in an underestimation of pCO_2 by up to approximately 150 μatm (Fig. 9c). Given that pCO_2 in Komuke Lagoon fluctuates between 0 μatm and 400 μatm, an underestimation of up to 150 μatm could lead to an overestimation of atmospheric CO_2 uptake by a factor of several times or more. Therefore, in highly enclosed shallow coastal areas like Komuke Lagoon, where river inflow causes TA variations of approximately 100 μmol kg^{-1}, changes in TA must be taken into account. Mechanistically, the reduction in TA due to riverine dilution shifts the carbonate equilibrium toward a higher fraction of aqueous CO_2. At a given DIC concentration, a lower TA value results in a higher pCO_2. This explains why assuming a constant TA value leads to an underestimation of pCO_2, thereby creating an artificial increase in the air-water CO_2 gradient and a significant overestimation of atmospheric CO_2 uptake. As an illustrative example, at DIC = 1700 μmol kg^{-1} and $T = 20$ °C, reducing TA from 2150 to 2000 μmol kg^{-1} increases pCO_2 from approximately 250 to 420 μatm (a factor of ~1.7), quantitatively consistent with Fig. 9c.

In addition to TA variability, we examined the sensitivity of the carbon budget to the variability of the river-water DIC endmember itself. Using the ±1 σ range of DIC_{river} (540 ± 110 μmol kg^{-1}), sensitivity simulations indicated that the corresponding change in each component of the summer-validated, annually-projected carbon budget (Table 2) remained within approximately ±12%, which is small relative to the dominant tidal exchange term (~66% of total CO_2 supply). This demonstrates that while the river DIC endmember is more temporally variable than the oceanic one, its variability does not materially affect the lagoon-integrated carbon budget. We note that flood events primarily affect the lagoon DIC through the dilution effect of large q_river, which is explicitly captured by the time-varying river discharge in Eq. (3), rather than through modulation of the river DIC concentration itself.

To quantify the uncertainty associated with the bottom dilution B, we performed sensitivity simulations in which B was perturbed by ±50% around its central value (Nagatomo et al., 2023; Nakayama et al., 2020). This range is chosen to span the lower end of the measurement uncertainties reported for bottom dilution in seagrass-dominated coastal sediments, which typically exceed ±70% under direct chamber incubations (e.g., Fan et al., 2024). Under the −50% and + 50% perturbations, the lagoon-averaged DIC changed by approximately −6.5 μmol kg^{-1} and 3.3 μmol kg^{-1}, respectively — small compared with the seasonal amplitude of ~500 μmol kg^{-1} and the endmember contrast of ~1440 μmol kg^{-1} (Section 3.1). The corresponding changes in the summer-validated, annually-projected atmospheric CO_2 uptake were approximately −4% and + 3%, respectively. These results indicate that although B contributes about 15% of the instantaneous DIC supply (Table 2), its uncertainty does not materially alter the main conclusions of this study regarding the dominance of tidal DIC supply and the role of eelgrass in DIC uptake. Regarding the seasonal correspondence between bottom dilution and the growth cycle of *Zostera marina*, B is expected to covary with sedimentary organic matter turnover, which is enhanced during periods of summer high water temperature. However, the steady-state B_0 formulation adopted here (Nagatomo et al., 2023) does not explicitly resolve this seasonality; the corresponding bias is conservatively bracketed by the ±50% sensitivity analysis.

Based on the computational results for one year in Komuke Lagoon, the CO_2 flux per unit surface area was calculated (Table 2 and Fig. 10). When the total contributions from factors increasing DIC—atmospheric uptake, river inflow, tidal exchange, and dilution from the bottom layer—were set to 100%, the largest supply of CO_2 to Komuke Lagoon was DIC transport from the Sea of Okhotsk via tides, accounting for approximately 66%. This was followed by dilution from the bottom layer and river inflow, with atmospheric CO_2 uptake making the most minor contribution. However, as this study did not model Dissolved Organic Carbon (DOC), and the dilution from the bottom layer includes DIC supply from DOC mineralization, the contribution of dilution from the lagoon bottom is likely overestimated (Lin et al., 2023). It was also found that *Zostera marina* absorbs approximately half of the CO_2 supplied to Komuke Lagoon.

Blue Carbon ecosystems, such as those dominated by *Zostera marina*,

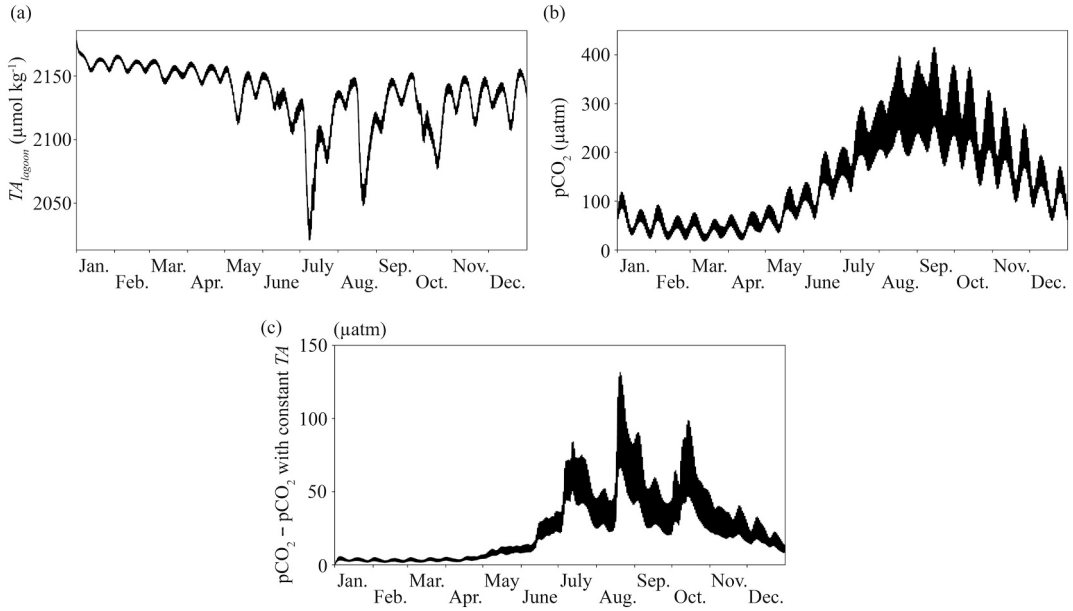


Fig. 9. Contribution of TA to DIC. (a) TA_{lagoon} in Komuke Lagoon in 2018. (b) pCO_2 with varied TA, (c) Difference of pCO_2 between varied and constant TA.

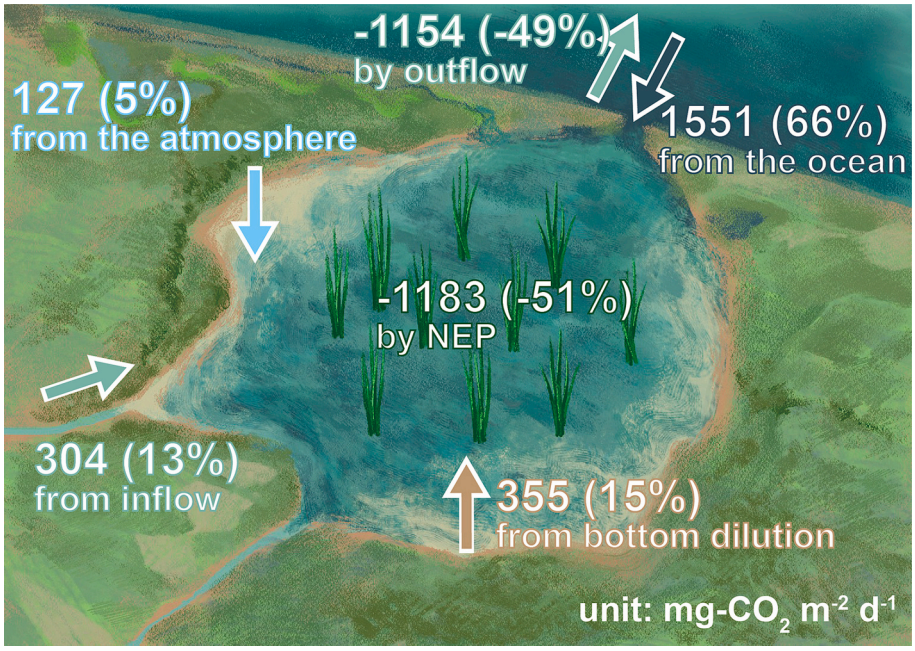


Fig. 10. Schematic diagram of the summer-validated, annually-projected carbon budget due to surface flux, inflow, tide, bottom dilution, *Zostera marina*, and outflow in 2018. The integration outside of summer (July–August) is reported as a model projection. Positive and negative values correspond to the increase and decrease in CO_2 in Komuke Lagoon.

are considered to indirectly absorb CO_2 from the water surface (Nellemann et al., 2009). In this study, the atmospheric CO_2 uptake attributed to *Zostera marina* accounted for 5.4% of the total CO_2 supply. Consequently, the atmospheric CO_2 uptake by *Zostera marina* was calculated to be 64 (=1183 × 5.4%) mg-CO_2 m^{-2} d^{-1}. These results demonstrate that *Zostera marina* absorbs only a minimal amount of CO_2 from the atmosphere; its primary role was revealed to be the reduction of CO_2 derived from open ocean and river waters. This partitioning implicitly assumes that DIC sources are well-mixed within the lagoon before uptake by eelgrass, which is consistent with the single-box framework.

This finding, that atmospheric CO_2 uptake accounts for only 5.4% of the total carbon supply, might at first glance appear to deviate from the general perception of blue carbon ecosystems as direct sinks for atmospheric CO_2. However, this reflects the specific hydrodynamic characteristics of Komuke Lagoon as a "restricted lagoon" with vigorous tidal exchange relative to its volume. Three site-specific factors explain the dominant role of tidal DIC supply over direct atmospheric exchange:

1. The lagoon is flushed approximately once per tidal cycle through the narrow 15-m inlet, resulting in a high tidal DIC load relative to the lagoon volume.
2. The adjacent Sea of Okhotsk water carries a high DIC concentration (~1980 μmol kg^{-1}), providing a large DIC load per unit tidal flux.
3. Although active eelgrass uptake maintains the lagoon pCO_2 well below atmospheric equilibrium, the physical magnitude of tidal transport remains orders of magnitude larger than the air-water flux. While direct atmospheric uptake is more dominant in open coastal settings, studies in other restricted or mangrove-dominated lagoons have similarly found that tidal DIC supply is the primary controller of the carbon budget. Crucially, our findings do not diminish the blue carbon significance of this ecosystem: *Zostera marina* still removes approximately half of the total DIC supplied from all sources (~1183 mg-CO_2 m^{-2} d^{-1}), representing a substantial carbon sink capacity that is consistent with the blue carbon paradigm.

4.4. Limitations of the single-box approach and generalizability

The conceptual DIC model adopted here intentionally simplifies Komuke Lagoon as a single well-mixed box. While the vertical profiles observed on August 8, 2018 (Fig. 5) and the strong tidal mixing through the 15-m inlet support this assumption on the whole-lagoon scale, localized processes are not resolved. In particular, (i) near-river-mouth zones may experience enhanced CO_2 outgassing due to the low-DIC freshwater endmember, (ii) benthic DIC release may vary spatially with sediment characteristics and eelgrass coverage, and (iii) transient partial stratification (as inferred from the July 23 surface–bottom DIC difference of ~110 μmol kg^{-1}) may temporarily trap bottom dilution within the meadow. These localized effects may introduce uncertainty in individual flux components, although the lagoon-integrated carbon budget presented in Table 2 is expected to be robust because the dominant endmember gradients are explicitly represented. A spatially resolved three-dimensional model would be required to quantify these localized processes and remains a subject for future work. In terms of the generalizability of our findings, Komuke Lagoon represents a typical "restricted lagoon" characterized by a narrow tidal inlet that acts as a dynamic filter, reducing tidal energy and water-level fluctuations (Kjerfve, 1994). This geomorphic stability is essential for maintaining the high density of eelgrass meadows observed in this study. While the relative importance of tidal exchange versus air-sea flux may vary in more open systems (e.g., leaky lagoons or estuaries with large tidal prisms), our findings provide a robust benchmark for the carbon budget of enclosed coastal lagoons where calm physical conditions promote significant biological carbon sequestration.

Although the river-water DIC endmember exhibits larger temporal variability than the oceanic endmember (110 vs. 20 μmol kg^{-1}), the sensitivity analysis in Section 4.3 confirmed that this variability does not substantially affect the lagoon-integrated carbon budget. Nevertheless, future studies incorporating high-frequency riverine DIC observations during flood events would further reduce uncertainty in the flood-time carbon budget.

The physical plausibility of the model under winter and spring conditions is supported by the calibrated DIC equation (Eq. 1). During winter (December–February), water temperatures in Komuke Lagoon

typically range from 0 to 5 °C. At such temperatures, both the exponential respiration term (NEPR) and the Gaussian temperature limitation term (NEPP) approach their minimum values, projecting near-zero NEP. The simulated winter DIC dynamics are therefore dominated by tidal exchange and river inflow, which is physically consistent with the known winter senescence of *Zostera marina* in temperate environments (Lee et al., 2007). During spring, the calibrated equation appropriately captures the progressive recovery of NEP as water temperature rises above the optimum range and photon flux density increases, reproducing the DIC decrease from January through late spring, which was simulated consistently across the three years for which the model was tested (2018 for the detailed carbon-budget analysis, and 2013 and 2019 as reproducibility and inter-annual consistency checks).

Although the conceptual DIC model was additionally tested against 2013 and 2019 as a reproducibility and inter-annual consistency check, the quantitative carbon-budget analysis was restricted to 2018 because simultaneous observations of DIC, TA, salinity and laboratory photosynthesis parameters are available only for that year. In addition, in situ observations of DIC, TA, and pCO_2 in Komuke Lagoon remain concentrated in summer across all three years. Continuous year-round observations — particularly during winter low-light conditions and spring peak-growth periods — are not yet available, and are identified as an essential next step. Accordingly, the simulated DIC dynamics outside of summer should be interpreted as model projections rather than directly validated results, and the annual carbon budget presented in Table 2 and Fig. 10 is best characterized as summer-validated and model-projected on an annual basis. All validation data are from summer (July–August). Winter and spring NEP projections should therefore be regarded as model extrapolations; their verification remains an open priority for future observational work. To address this gap, we plan to conduct year-round, high-frequency observations of DIC, TA and pCO_2 in Komuke Lagoon, ideally complemented by under-ice light and temperature logging and by sediment incubations capturing the seasonal variation of benthic carbon release.

5. Conclusion

A study on the carbon budget was conducted using a conceptual DIC model targeting Komuke Lagoon, which is dominated by *Zostera marina*. First, to model the release and uptake of CO_2 via the respiration and photosynthesis of *Zostera marina*, we utilized results from outdoor experiments conducted in 2018 and 2023. Following Ranjbar et al. (2024), we proposed a new DIC equation that accounts for the effect of water temperature on CO_2 uptake during photosynthesis. By applying this DIC equation to the box model and accounting for river inflow, tidal exchange, bottom dilution, air-sea exchange, and uptake by *Zostera marina*, the results of field observations conducted in July and August 2018 were successfully reproduced. The DIC equation and the conceptual DIC model were then applied to the calendar year 2018 for the detailed quantitative analysis of the summer-validated carbon budget, integrated over the simulated calendar year, and the partitioning of the contributions of river inflow, tidal exchange, bottom dilution, air–water CO_2 flux, and eelgrass metabolism. The same model was additionally applied to 2013 and 2019 as a reproducibility test of the calibrated parameters and as a check of the inter-annual consistency of the model skill against the available summer observations; in both years the observed summer DIC was reproduced within the observational uncertainty, while the detailed carbon-budget partitioning reported below refers exclusively to 2018. The simulated DIC dynamics outside of summer are reported as model projections only. The effect of DIC uptake by *Zostera marina* was found to be significant; disregarding it resulted in an overestimation of approximately 300 μmol kg^{-1}. A major feature of the box model proposed in this study is the inclusion of Total Alkalinity (TA) modeling. It was found that ignoring variations in TA led to an underestimation of pCO_2 by up to 150 μatm. Given that pCO_2 fluctuations in Komuke Lagoon range from 0 to 400 μatm, assuming a constant TA value could lead to an overestimation of atmospheric CO_2 uptake by a factor of several times or more. Therefore, when estimating the CO_2 flux between the atmosphere and the water surface, it is necessary to incorporate variations in TA. In 2018, tidal exchange had the largest impact on DIC in the waters of Komuke Lagoon, contributing 66%, whereas the influence of air–sea flux was the smallest, accounting for approximately 5.4%. In summary, while the primary carbon source for *Zostera marina* in this restricted lagoon is derived from tidal and riverine DIC rather than direct atmospheric absorption, the eelgrass metabolism plays a vital role in maintaining low pCO_2 levels. This process mediates the removal of atmospheric CO_2 on a lagoon-integrated basis, highlighting the importance of considering hydrodynamic connectivity when evaluating the carbon sequestration functions of temperate blue carbon ecosystems.

CRediT authorship contribution statement

Y. Fukuda: Writing – review & editing, Writing – original draft, Visualization, Validation, Software, Formal analysis. **M. Maruyama:** Visualization, Investigation. **Y. Peng:** Visualization. **H. Yoneda:** Visualization. **K. Tada:** Conceptualization. **K. Nakayama:** Writing – review & editing, Writing – original draft, Visualization, Validation, Supervision, Software, Resources, Project administration, Methodology, Investigation, Funding acquisition, Formal analysis, Data curation, Conceptualization.

Funding sources

This work was supported by the Japan Society for the Promotion of Science under grant nos. 25H00408, and 23K22871.

Declaration of competing interest

The authors declared that they have no competing interests.

Data availability

Data will be made available on request.

References

Beca-Carretero, P., Olesen, B., Marbà, N., Krause-Jensen, D., 2018. Response to experimental warming in northern eelgrass populations: comparison across a range of temperature adaptations. Mar. Ecol. Prog. Ser. 589, 59–72.
Burkholz, C., Duarte, C.M., Garcias-Bonet, N., 2019. Thermal dependence of seagrass ecosystem metabolism in the Red Sea. Mar. Ecol. Prog. Ser. 614, 79–90.
Cabello-Pasini, A., Muñiz-Salazar, R., Ward, D.H., 2003. Annual variations of biomass and photosynthesis in Zostera marina at its southern end of distribution in the North Pacific. Aquat. Bot. 76, 31–47.
Dennison, W.C., Aller, R.C., Alberte, R.S., 1987. Sediment ammonium availability and eelgrass (Zostera marina) growth. Mar. Biol. 94, 469–477.
Drew, E.A., 1979. Physiological aspects of primary production in seagrasses. Aquat. Bot. 7, 139–150.
Duarte, C.M., Losada, I.J., Hendriks, I.E., Mazarrasa, I., Marbà, N., 2013. The role of coastal plant communities in the global carbon cycle. Biogeosciences 10 (12), 7955–7976.
Fan, L.-F., Kang, E.-C., Natividad, M.B., Hung, C.-C., Shih, Y.-Y., Huang, W.-J., Chou, W.-C., 2024. The Role of Benthic TA and DIC Fluxes on Carbon Sequestration in Seagrass Meadows of Dongsha Island. J. Mar. Sci. Eng. 12 (11), 2061.
Fourqurean, J.W., Duarte, C.M., Kennedy, H., Marbà, N., Holmer, M., Mateo, M.A., Apostolaki, E.T., Kendrick, G.A., Krause-Jensen, D., McGlathery, K.J., Serrano, O., 2012. Seagrass ecosystems as a globally significant carbon stock. Nat. Geosci. 5, 505–509.
Goodman, J.L., Moore, K.A., Dennison, W.C., 1995. Photosynthetic responses of eelgrass (Zostera marina L.) to light and sediment sulfide in a shallow barrier island lagoon. Aquat. Bot. 50, 37–47.
Hellweger, F.L., Kravchuk, E.S., Novotny, V., Gladyshev, M.I., 2008. Agent-based modeling of the complex life cycle of a cyanobacterium (Anabaena) in a shallow reservoir. Limnol. Oceanogr. 53, 1227–1241.
Herzka, S., Dunton, K., 1998. Light and carbon balance in the seagrass Thalassia testudinum: evaluation of current production models. Mar. Biol. 132, 711–721.

Holmer, M., Bondgaard, E.J., 2001. Photosynthetic and growth response of eelgrass to low oxygen and high sulfide concentrations during hypoxic events. Aquat. Bot. 70, 29–38.
Intergovernmental Panel on Climate Change (IPCC), 2007. Climate Change 2007: The Physical Science Basis. Contribution of Working Group I to the Fourth Assessment Report of the Intergovernmental Panel on Climate Change. IPCC, Geneva, Switzerland.
Intergovernmental Panel on Climate Change (IPCC), 2013. Climate Change 2013: The Physical Science Basis. Contribution of Working Group I to the Fifth Assessment Report of the Intergovernmental Panel on Climate Change. IPCC, Geneva, Switzerland.
Kjerfve, B., 1994. Coastal lagoons. In: Kjerfve, B. (Ed.), Coastal Lagoon Processes, 60. Elsevier Oceanography Series, pp. 1–8.
Lee, K.S., Park, S.R., Kim, Y.K., 2007. Effects of irradiance, temperature, and nutrients on growth dynamics of seagrasses: A review. J. Exp. Mar. Biol. Ecol. 350, 144–175.
Lee, K.-S., Park, S.R., Kim, J.-B., 2005. Production dynamics of the eelgrass, Zostera marina in two bay systems on the south coast of the Korean peninsula. Mar. Biol. 150, 1091–1108.
Lee, S.Y., Kim, J.B., Lee, S.M., 2006. Temporal dynamics of subtidal Zostera marina and intertidal Zostera japonica on the southern coast of Korea. Mar. Ecol. 27, 133–144.
Lin, H.C., Nakayama, K., Tsai, J.W., Chiu, C.Y., 2023. Conceptual models of dissolved carbon fluxes in a two-layer stratified lake: interannual typhoon responses under extreme climates. Biogeosciences 20, 4359–4376.
Macreadie, P.I., Anton, A., Raven, J.A., Beaumont, N., Connolly, R.M., Friess, D.A., Kelleway, J.J., Kennedy, H., Kuwae, T., Lavery, P.S., Lovelock, C.E., Smale, D.A., Apostolaki, E.T., Atwood, T.B., Baldock, J., Bianchi, T.J., Chmura, G.L., Eyre, B.J., Fourqurean, J.W., Hall-Spencer, J.M., Huxham, M., Hendriks, I.E., Krause-Jensen, D., Laffoley, D., Luisetti, T., Marbà, N., Masqué, P., McGlathery, K.J., Megonigal, J.P., Murdiyarso, D., Russell, B.D., Santos, R., Serrano, O., Silliman, B.R., Smith, J.R., Smoak, J.P., Spiers, S.J., Stoddart, M., Swanson, T., Thompson, R., Valiela, I., Duarte, C.M., 2019. The future of Blue Carbon science. Nat. Commun. 10 (1), 3998.
Marsh Jr., J.A., Dennison, W.C., Alberte, R.S., 1986. Effects of temperature on photosynthesis and respiration in eelgrass (Zostera marina L.). J. Exp. Mar. Biol. Ecol. 101, 257–267.
Maruyama, M., Nakayama, K., Komai, K., Peng, Y., Sakaguchi, J., Tada, K., 2024. Impact of eelgrass on carbon capture in Lake Komuke. J. JSCE Ser. B2 (Coastal Eng.) 80, 24–17231.
Mizushima, T., 1985. Seasonal changes in standing crop and production of eelgrass (Zostera marina L.) in Notsuke Bay, eastern Hokkaido. In: Sci. Rep. Hokkaido Fish. Exp. Stn., No 27, pp. 111–118 in Japanese with English abstract.
Moore, K.A., Neckles, H.A., Orth, R.J., 1996. Zostera marina (eelgrass) growth and survival along a gradient of nutrients and turbidity in the lower Chesapeake Bay. Mar. Ecol. Prog. Ser. 142, 247–259.
Nagatomo, K., Nakayama, K., Komai, K., Matsumoto, H., Watanabe, K., Kubo, A., Tada, K., Maruya, Y., Yajima, H., Tsai, J.W., Lin, H.C., Vilas, M.P., Hipsey, M.R., 2023. A spatially integrated dissolved inorganic carbon (SiDIC) model for aquatic ecosystems considering submerged vegetation. J. Geophys. Res. Biogeosci. 128 (2).
Nakayama, K., Sivapalan, M., Sato, C., Furukawa, K., 2010. Stochastic characterization of the onset of and recovery from hypoxia in Tokyo Bay, Japan: Derived distribution analysis based on “strong wind” events. Water Resour. Res. 46, W12532.
Nakayama, K., Komai, K., Tada, K., Lin, H.C., Yano, S., Watanabe, K., Hipsey, M.R., Tsai, J.W., 2020. Modelling dissolved inorganic carbon considering submerged aquatic vegetation. Ecol. Model. 431, 109188.
Nakayama, K., Kawahara, Y., Kurimoto, Y., Tada, K., Lin, H.C., Hung, M.C., Hsueh, M.L., Tsai, J.W., 2022. Effects of oyster aquaculture on carbon capture and removal in a tropical mangrove lagoon in southwestern Taiwan. Sci. Total Environ. 838, 156460.
Nellemann, C., Corcoran, E., Duarte, C.M., Valdes, L., DeYoung, C., Fonseca, L., Grimsditch, G., 2009. Blue Carbon. A Rapid Response Assessment. United Nations Environmental Programme, GRID-Arendal, Birkeland.
Olesen, B., Sand-Jensen, K., 1993. Seasonal acclimatization of eelgrass Zostera marina growth to light. Mar. Ecol. Prog. Ser. 94, 91–99.
Palacios, S.L., Zimmerman, R.C., 2007. Response of eelgrass Zostera marina to CO2 enrichment: possible impacts of climate change and potential for remediation of coastal habitats. Mar. Ecol. Prog. Ser. 344, 1–13.
Prokopkin, I., Gubanov, V., Gladyshev, M., 2006. Modelling the effect of planktivorous fish removal in a reservoir on the biomass of cyanobacteria. Ecol. Model. 190, 419–431.
Ranjbar, M.H., Hamilton, D.P., Pace, M.L., Etemad-Shahidi, A., Carey, C.C., Helfer, F., 2024. Individual-based modelling of adaptive physiological traits of cyanobacteria: Responses to light history. Ecol. Model. 495, 110803.
Sato, C., Nakayama, K., Furukawa, K., 2012. Contributions of wind and river effects on DO concentration in Tokyo Bay. Estuar. Coast. Shelf Sci. 109, 91–97.
Short, F.T., Neckles, H.A., 1999. The effects of global climate change on seagrasses. Aquat. Bot. 63, 169–196.
Staehr, P.A., Borum, J., 2011. Seasonal acclimation in metabolism reduces light requirements of eelgrass (Zostera marina). J. Exp. Mar. Biol. Ecol. 407, 139–146.
Tokoro, T., Hosokawa, S., Miyoshi, E., Tada, K., Watanabe, K., Montani, S., Kayanne, H., Kuwae, T., 2014. Net uptake of atmospheric CO2 by coastal submerged aquatic vegetation. Glob. Chang. Biol. 20, 1873–1884.
Touchette, B.W., 1999. Physiological and developmental responses of eelgrass (*Zostera marina* L.) to increases in water-column nitrate and temperature. Ph.D. Dissertation. North Carolina State University, Raleigh, NC.
Watanabe, K., Kuwae, T., 2021. An unintended ecological benefit from human intervention: The enhancement of carbon storage in seagrass meadows. J. Appl. Ecol. 58, 2441–2452.
Watanabe, M., Nakaoka, M., Mukai, H., 2005. Seasonal variation in vegetative growth and production of the endemic Japanese seagrass *Zostera asiatica*: a comparison with sympatric *Zostera marina*. Bot. Mar. 48, 266–273.
Zeebe, R.E., Wolf-Gladrow, D., 2001. Equilibrium. In: CO2 in Seawater: Equilibrium, Kinetics, Isotopes. Elsevier, Amsterdam, pp. 1–83.
Zimmerman, R.C., Reguzzoni, J.L., Alberte, R.S., 1995. Eelgrass (Zostera marina L.) transplants in San Francisco Bay: role of light availability on metabolism, growth and survival. Aquat. Bot. 51, 67–86.
Zimmerman, R.C., Kohrs, D.G., Steller, D.L., Alberte, R.S., 1997. Impacts of CO2 enrichment on productivity and light requirements of eelgrass. Plant Physiol. 115, 599–607.